Journal of Materials Chemistry C

ROYAL SOCIETY OF CHEMISTRY

PAPER

View Article Online
View Journal | View Issue

Cite this: J. Mater. Chem. C, 2022, 10, 7469

A Zr-MOF nanoflower sensor and its mixed-matrix membrane for the highly sensitive detection of nitroaromatics†

Hui Xu,*[a] Fangyuan Zhong,[b] Faqiang Chen,[a] Tian-Xiang Luan,[c] Peizhou Li,*[c] Shiqing Xu*[a] and Junkuo Gao*[b]

Received 7th March 2022,
Accepted 21st April 2022

DOI: 10.1039/d2tc00920j

rsc.li/materials-c

A new luminescent metal–organic framework nanoflower material **CJLU-1** ($Zr_6(\mu_3\text{-}O)_4(\mu_3\text{-}OH)_4(OH)_6(TCA)_2(H_2O)_6$) ($H_3TCA$ = tri-carboxylic acids 4,4′,4″-nitrilotribenzoic acid) has been realized for the highly sensitive sensing of nitroaromatic molecules with fast response. **CJLU-1** consists of six-connected Zr6 clusters and three-connected TCA ligands, and forms a 2D layered porous structure. The intrinsic 2D layered crystal structure and the optimal synthesis method create an ordered nanoflower structure constructed using ultrathin nanosheets. The highly dispersive nature and the controllable nanoflower structure with highly accessible active sites on the surface enable them to have full contact with the targeted analytes, which leads to superior sensing performance, with a high detection limit of 0.362 μM (≈83 ppb) toward 2,4,6-trinitrophenol (PA), strong anti-interference and a fast response within seconds. Moreover, a novel sensing platform, **CJLU-1** mixed-matrix membranes (MMMs), is established by hybridization of the **CJLU-1** nanoflower and cellulose acetate polymer, and exhibits desirable vapor sensing towards nitroaromatic molecules. This work contributes to the development of controllable nanostructured MOF probes and MOF-based MMMs as a novel sensing platform with superior mechanical strength, flexibility and sensitivity towards practical chemical sensing applications.

Introduction

Metal–organic framework materials (MOFs) are porous crystalline materials assembled from metal ions/metal clusters and organic ligands, and have shown many potential applications including gas storage and separation, heterogeneous catalysis, drug delivery, luminescence *etc.*[1–7] The differential recognition/binding sites, tunable pore sizes and functionalized pore surfaces have made MOFs important sensing materials.[8–10] An efficient luminescent sensing material requires high sensitivity, high selectivity, anti-interference, fast response time *etc.*[11,12] Among them, the realization of high sensitivity requires sensing materials to be in close contact with analytes.[13–15] The porous nature of MOFs facilitates adsorbing and pre-concentrating the analytes, increasing the possibility of host–guest interactions and improving the sensitivity.[11,16,17] Moreover, the controllable nanostructure is also an important factor to improve the sensitivity. The unique nanostructure of MOFs endows them with larger surface area, more exposed functional sites, increasing the feasibility of adequate contact with the analytes and improved sensitivity.[18–22] Two-dimensional (2-D) MOF nanosheets, an emerging type of 2D material that possess good dispersibility, large surface areas and abundant accessible sites, have shown great potential in luminescence sensing.[23–31] There are some pioneering studies showing the superior performance of 2D MOF nanosheets in the construction of fluorescent sensors.[32–35] However, work on MOFs with controllable nanostructures for luminescence sensing is still relatively scarce.

On the other hand, currently the sensing work of MOFs is mainly based on MOF powder or nanoscale MOFs dispersed in liquid media, which suffers from inconvenience in the recycling.[9] And for further application, MOF samples need to be fabricated into thin films or membranes.[36,37] MOF-based mixed-matrix membranes (MMMs) have been well demonstrated to be promising candidates. The MOF-based MMMs

[a] Key Laboratory of Rare Earth Optoelectronic Materials and Devices of Zhejiang Province, Institute of Optoelectronic Materials and Devices, Collage of Optical and Electronic Technology, China Jiliang University, Hangzhou 310018, People's Republic of China. E-mail: huixu@cjlu.edu.cn, shiqingxu75@163.com
[b] Institute of Functional Porous Materials, The Key laboratory of Advanced Textile Materials and Manufacturing Technology of Ministry of Education, School of Materials Science and Engineering, Zhejiang Sci-Tech University, Hangzhou 310018, P. R. China. E-mail: jkgao@zstu.edu.cn
[c] School of Chemistry and Chemical Engineering, Shandong University, No. 27 Shanda South Road, Ji'nan, 250100, People's Republic of China. E-mail: pzli@sdu.edu.cn

† Electronic supplementary information (ESI) available: Supporting figures. See DOI: https://doi.org/10.1039/d2tc00920j

combine the superior properties of novel porous MOFs as well as flexibility and easy processability of traditional polymeric membranes.[38–40] Compared with the pure MOF thin films, which usually have to be delicately grown on substrates, MOF-based MMMs exhibit superior mechanical properties, more flexibility, easier processability and lower cost. Currently, the applications of MOF-based MMMs are evaluated in gas separation, pervaporation, nanofiltration, and sensors.[41–44] However, the studies of MOF-based MMMs for luminescence sensing are still at the early stage, and the use of MOF-based MMMs for nitroaromatic sensing has not been established yet.[45] By incorporating luminescent MOFs into polymeric membranes, MOF-based MMMs exhibit efficient luminescence properties.[46,47] The combination of structurally designable MOFs and flexible porous polymeric membranes offers unique and effective integration in specific sensing applications. Furthermore, MOF particles are uniformly distributed and closely enwrapped in the polymeric matrix, which enables good gas permeation flux and facilitates a full contact between MOF particles and analytes to enhance the detection sensitivity.[48]

Herein, we innovatively explored a new nanoflower-like **CJLU-1** MOF ($Zr_6(\mu_3\text{-}O)_4(\mu_3\text{-}OH)_4(OH)_6(TCA)_2(H_2O)_6$) ($H_3TCA$= tri-carboxylic acids 4,4′,4″-nitrilotribenzoic acid) luminescent sensing material with a hexanuclear Zr cluster and a 2D porous crystal structure, and the nanoflowers were constructed using two-dimensional ultrathin MOF nanosheets. By utilizing the strong electron donating ability of the nitrogen atom in the center of the triphenylamine ligand and uniform nanoflower structure, the **CJLU-1** nanoflower material exhibited superior sensing properties towards electron deficient nitroaromatics with ppb-level sensitivity. Furthermore, the **CJLU-1** nanoflower material was incorporated into a cellulose acetate matrix to prepare hybrid sensing membranes (**CJLU-1** MMMs) (as shown in Scheme 1). The **CJLU-1** MMMs inherited porosity and sensing functionality from the MOF as well as the flexibility and easy processability from the cellulose acetate matrix, and exhibited efficient and recyclable detection of nitroaromatics.

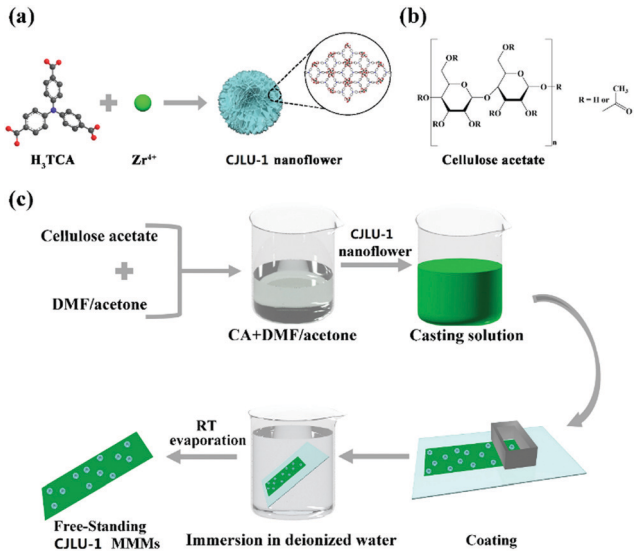

Scheme 1 Schematic illustration of the preparation of **CJLU-1** MMMs.

Results and discussion

The reaction of $ZrCl_4$ with the tritopic carboxylate ligand H_3TCA[49] in DMF and HCl formed a new porous Zr-MOF **CJLU-1**. Interestingly, the *in situ* hydrothermal method easily yielded high-quality **CJLU-1** nanoflowers. However the crystal size of the synthesized Zr-MOF sample was too small, making it very difficult to directly determine the crystal structure from single-crystal diffraction measurements. Therefore, powder X-day diffraction analysis and structure simulation were utilized to elucidate the MOF structure. Based on the nature of the triple symmetry of the TCA ligand and the geometry of the commonly formed hexanuclear Zr_6 cluster as well as the results of PXRD measurements, a (3,6)-connected framework in *kgd* topology with an eclipsed AA stacking model was built using the Materials Studio software package (Fig. 1). The several relatively intense peaks at 5.93°, 10.16°, 21.12°, and 26.79° observed from the experimental PXRD pattern of the synthesized Zr-MOF were assigned to the diffractions of (100), (110), (130), and (401) planes, respectively. After Pawley refinements (Fig. 1), **CJLU-1** was indexed to a trigonal $P\bar{3}$ space group with cell parameters $a = b = 17.1740$ Å, $c = 7.0100$ Å, $\alpha = \beta = 90°$, $\gamma = 120°$ and satisfactory residual values $R_p = 6.25\%$ and $R_{wp} = 8.63\%$. **CJLU-1** is a two-dimensional (2D) layered framework. Six Zr atoms are joined into a six connected $Zr_6(\mu_3\text{-}O)_4(\mu_3\text{-}OH)_4(OH)_6$ octahedron subunit, and then the Zr_6-octahedron clusters are connected by TCA ligands to form a 2D layered porous structure (Fig. 1b and Fig. S1, ESI†). The Zr_6-octahedron cluster is bridged by 4 μ_3-O and 4 μ_3-OH groups to form an octahedron subunit, which are further linked with six TCA ligands. **CJLU-1** has one-dimensional pores of about 3.5×4.0 Å^2 along the c axis and a pore volume of 0.205 cm^3 g^{-1}. The comparison of the PXRD patterns between the experimental one and the one generated from the simulated structure reveals that they are consistent with each other, which also confirmed the phase purity of the synthesized sample of **CJLU-1** (Fig. S2, ESI†). The intrinsic 2D layered crystal structure and the optimal synthesis method create ordered nanoflower structures constructed using ultrathin nanosheets. The SEM and TEM measurements reveal that the obtained

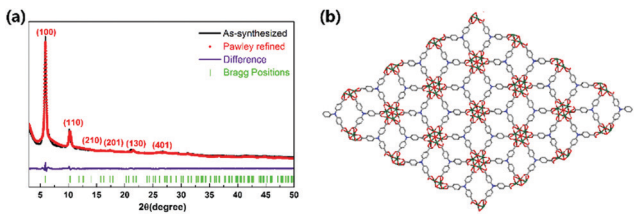

Fig. 1 (a) The PXRD patterns from the experimental measurements of the synthesized MOF (black curve) and the simulated structure in a (3,6)-connected framework with an eclipsed AA stacking model. (b) Simulated frameworks constructed using the TCA ligands and hexanuclear Zr_6 clusters.

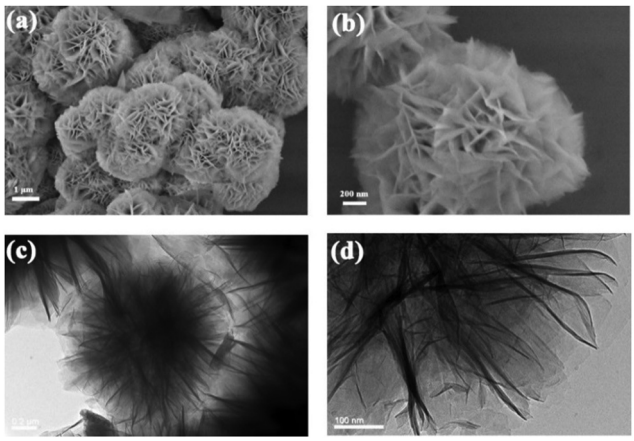

Fig. 2 (a and b) The SEM images of **CJLU-1**; (c and d) the TEM images of **CJLU-1**.

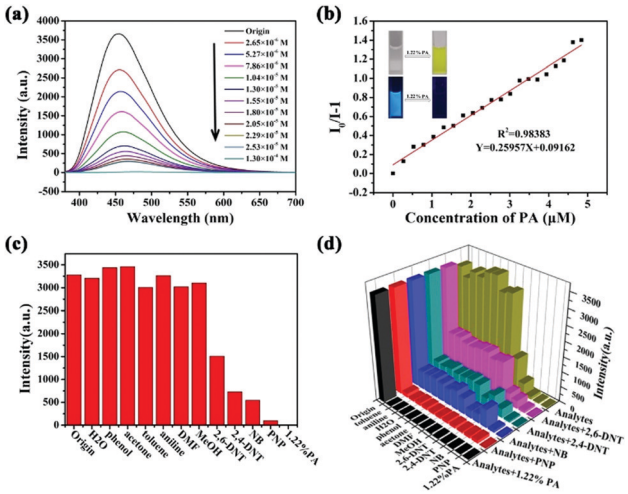

Fig. 3 (a) The PL spectrum of **CJLU-1** nanoflowers with different amounts of PA; (b) S–V plots of PA; inset: the picture above is a photo of **CJLU-1** ethanol solution before and after adding 50 μL of 1.22% PA, under nature light and UV light at 365 nm, respectively; (c) the 454 nm emission intensity of **CJLU-1** ethanol solution with 2.5×10^{-3} M different small organic molecule (the concentration of PA was 1.3×10^{-3} M); and (d) the emission intensity of **CJLU-1** ethanol solution with 2.5×10^{-3} M nitro-aromatic molecules (the concentration of PA was 1.30×10^{-3} M) in the presence of 2.5×10^{-3} M other small organic molecules.

CJLU-1 exhibits uniform nanoflower morphologies with a typical diameter of 3 μm. The nanoflowers are constructed using dozens of interpenetrated ultrathin 2D nanosheets with smooth surfaces. The lateral dimension of the nanosheets reached up to micrometers and their thicknesses were less than 10 nm (Fig. 2).

The above nanoflower feature of **CJLU-1** encouraged us to examine its potential application in luminescence sensing. The solid state **CJLU-1** exhibits photoluminescence (PL) properties with a fluorescence peak at 454 nm (Fig. S3, ESI†), which is slightly blue-shifted from the fluorescence peak of the free ligand H_3TCA located at 458 nm (Fig. S3, ESI†). The PL properties of **CJLU-1** could be attributed to the fluorescence of ligand H_3TCA in the framework. The **CJLU-1** nanoflower material can be easily dispersed in ethanol to form a uniform suspension solution, and exhibits a strong PL emission peak located at 454 nm (Fig. S4, ESI†).

The strong emission of the **CJLU-1** nanoflower material encouraged us to examine its potential application in liquid-phase fluorescence detection of nitroaromatic molecules. The addition of a small amount of organic small molecules (5×10^{-6} mol, the amount of PA is 2.7×10^{-6} mol) has different effects on the luminescence intensity of the dispersed nanoflower in ethanol (Fig. 3c). Analytes, such as methanol, water, phenol, acetone, toluene, aniline, and *N*,*N*-dimethylformamide (DMF), do not substantially affect the luminescence intensity of **CJLU-1** nanoflower ethanol solution, while the nitroaromatic molecules have a significant quenching effect on **CJLU-1** nanoflowers, indicating that the **CJLU-1** nanoflower material can be used to detect small amounts of nitroaromatic molecules. It is interesting that the **CJLU-1** nanoflower material shows different quenching effects for different nitroaromatic molecules. The quenching effect of 2,4,6-trinitrophenol (PA) and *p*-nitrophenol (PNP) on MOF solution is significantly higher than that of nitrobenzene (NB), 2,4-dinitrotoluene (2,4-DNT) and 2,6-dinitrotoluene (2,6-DNT) (Fig. 3c). The quenching effect of different nitroaromatic molecules decreased in the order PA > PNP > NB > 2,4-DNT > 2,6-DNT. In particular, PA has the strongest quenching effect on **CJLU-1** nanoflower solution. The addition of only 2.65 μM PA can efficiently quench the nanoflowers' fluorescence; the addition of 7.86 μM PA can quench the intensity to less than half of the original fluorescence intensity; and the addition of 25.3 μM PA can almost completely quench the nanoflowers' fluorescence (Fig. 3a). The **CJLU-1** nanoflower material exhibits superior sensing properties toward PA, with the detection limit reaching 0.362 μM (≈83 ppb) (Fig. S9, ESI†), clearly indicating the excellent potential of the **CJLU-1** controllable nanostructure approach in the precise detection of PA. The highly dispersive nature and the ultrathin nanosheets inside provide highly accessible active sites on their surface, which leads to adequate contact with the targeted nitroaromatic molecules and high detection sensitivity. Noticeably, the **CJLU-1** nanoflower material displays a linear response with PA concentration in the low concentration range. The quenching efficiency of PA can be quantitatively explained by using the Stern–Volmer equation. The relationship between $(I_0/I - 1)$ and the concentration of PA was calculated using the Stern–Volmer equation ($I_0/I = 1 + K_{sv}[M]$) and plotting the S–V plots, where I_0 and I are the fluorescence intensities of **CJLU-1** nanoflowers and **CJLU-1** nanoflower material with PA at a concentration of $[M]$, and K_{sv} is the quenching coefficient. As shown in Fig. 3b, the estimated Stern–Volmer constant is as high as 2.60×10^5 M^{-1}.

To gain more understanding of the detection selectivity towards nitroaromatic molecules in the presence of other analytes, the anti-interference experiment was carried out. The result shows that the presence of other analytes (such as toluene, aniline, water, phenol, acetone, DMF and MeOH)

basically has little interference on the luminescence intensity of the **CJLU-1** nanoflower ethanol solution with nitroaromatic molecules, indicating the high nitroaromatic molecule selectivity of **CJLU-1** in the concurrent presence of other analytes (Fig. 3d).

In addition, the fluorescence intensity of **CJLU-1** at 455 nm was measured as a function of time after the addition of 2.65×10^{-4} M PA. As shown in Fig. S10 (ESI†), the fluorescence intensity was completely quenched after the addition of PA within 20 seconds, and kept almost the same for the remaining time, indicating the ability of fast-response detection of PA. The dispersible nature and highly exposed surface of the MOF nanoflower materials have enabled a close contact between the MOF nanoflowers and the organic molecules, which leads to fast response of luminescence sensing, thus providing a promising strategy to implement MOF nanoflowers as fast-response sensing materials.

The luminescence of the **CJLU-1** nanoflower results from the fluorescence of the coordinated ligand H_3TCA in the framework. The addition of the nitroaromatics resulted in the fluorescence quenching of **CJLU-1**, while the powder XRD patterns of **CJLU-1** with the addition of a large amount (10^{-3} M) of nitroaromatics are identical with that of the original one (Fig. S11, ESI†), indicating that the crystal structure of **CJLU-1** remained stable in different chemical environments. The FT-IR spectra of **CJLU-1** immersed in different nitroaromatic solutions were consistent with those of the original **CJLU-1**, indicating that there was no coordination with the analytes and MOFs (Fig. S12, ESI†). The quenching effect of the nitroaromatics on **CJLU-1** was evaluated by the fluorescence decay time of **CJLU-1**. As shown in Fig. S13 (ESI†) and Table S2, (ESI†) the nitroaromatics had no significant effect on the fluorescence lifetime of **CJLU-1**, demonstrating that there is no coordination between **CJLU-1** and the analytes.

Based on previous pioneering work on MOF-based sensing materials for nitroaromatic detection,[50] the quenching mechanism process mainly includes photoinduced electron transfer (PET) and fluorescence resonance energy transfer (FRET). The electronic properties of the MOFs are crucial to their sensing behaviors. Considering the electron-withdrawing feature of the nitroaromatic molecules, the rational design of electron donating MOFs can effectively promote the electron transfer between the MOFs and the targeted nitroaromatic molecules, and a similar mechanism has been widely applied in previous work.[11,51] The nitrogen atom in the center of the triphenylamine ligand has strong electron donating ability, thus we speculate that the excited electrons at the conductive band of the **CJLU-1** nanoflowers will easily migrate to the LUMO of the nitroaromatic molecules upon excitation and then followed a non-radiative relaxation, leading to a fluorescence quenching process. Besides, compared with other nitroaromatics, the absorption spectra of the PA and PNP effectively overlap with the emission spectrum of **CJLU-1** (Fig. S14, ESI†), which facilitates the energy transfer between the analytes and MOFs, and induces a dramatic decrease in the fluorescence intensity of **CJLU-1**.

For practical application, **CJLU-1**-based MMMs were fabricated. MOF-based MMMs utilize MOFs as inorganic filler components in polymer membranes, and preserve not only the porosity, chemical tunability, and functionality of the MOFs, but also stand in the form of a stable, flexible, freestanding membrane. Cellulose acetate is widely utilized as a polymer base material for the membrane because of its biocompatibility, nontoxicity and low cost features. Also the presence of acidic and carbonyl groups in the cellulose acetate structure helps in binding with functional additives, and improves mixed matrix membranes (MMMs) performance.[52] The **CJLU-1** MOF-based MMMs can be readily prepared by the combination of MOFs into the acetone/DMF solution of cellulose acetate to form casting solution. After casting onto a glass plate using a wiper and being immersed into deionized water and dried at room temperature, freestanding **CJLU-1** MOF based MMMs can be obtained.

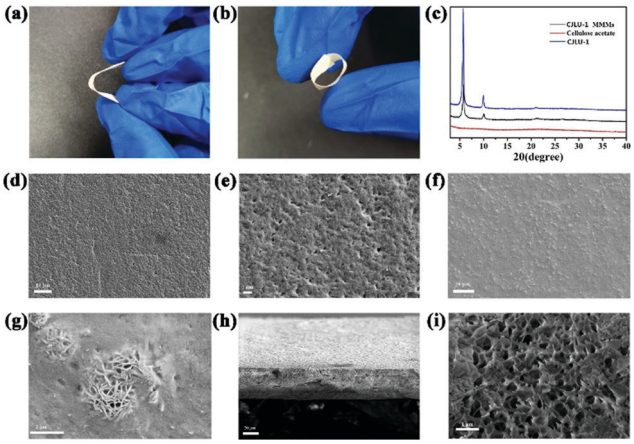

Fig. 4 (a and b) Different views of **CJLU-1** MMMs under mechanical stress; (c) PXRD of **CJLU-1**, **CJLU-1** MMMs and cellulose acetate membrane; (d and e) SEM images of the cellulose acetate membrane; (f and g) SEM images of **CJLU-1** MMMs; and (h and i) SEM images of the cross section of **CJLU-1** MMMs.

The delaminated **CJLU-1** MMM is free-standing, mechanically robust, pliable, and free of macroscopic defects (Fig. 4a and b). The morphology of **CJLU-1** MMMs was observed by SEM using a pure cellulose acetate membrane as a reference (Fig. 4d–i). At low magnifications, both the pure cellulose acetate membrane and the **CJLU-1** MMMs exhibit smooth and neat surfaces, and the MOF particles are uniformly distributed in **CJLU-1** MMMs (Fig. 4d and f). And at high magnifications, the pure cellulose acetate membrane exhibits crosslinking and macro-porous morphology (Fig. 4e). For the **CJLU-1** MMMs, the **CJLU-1** nanoflowers are closely embedded and partially exposed in the cellulose acetate matrix (Fig. 4g), which provides both strong MOF–polymer adhesion and adequate MOF–environment contact, and is very important for further sensing application. The cross-sectional SEM also indicates the smooth surface and the macro-porous feature of the **CJLU-1** MMMs, and the thickness of the membrane was approximately 40 μm (Fig. 4h and i).

The macro-porous feature of the membrane facilitates the diffusion of the analytes and helps in the sufficient contact between the analytes and MOF both inside and on the surface of the membrane, and thus improves the sensing performance.

As shown in Fig. 4c, PXRD of **CJLU-1** MMMs was carried out. The pure cellulose acetate membrane was amorphous, evidenced by a broad peak between 2θ of 15 and 30°.[53–55] With the addition of **CJLU-1**, the characteristic peak of **CJLU-1** appears. Because of the strong characteristic peak intensity of **CJLU-1**, the diffraction peak of the cellulose acetate membrane is almost negligible. These results indicate that the crystallinity and structural features of **CJLU-1** remain well in the cellulose acetate membrane. In addition, the loading of the cellulose acetate membrane based on MOFs was studied by thermogravimetric analysis, and the loading of **CJLU-1** was calculated to be as high as 39.53% (Fig. S15, ESI†). The N_2 adsorption–desorption isotherms of **CJLU-1**, **CJLU-1** MMMs and the pure cellulose acetate membrane at 77 K were obtained to confirm their specific surface areas. The BET of **CJLU-1**, **CJLU-1** MMMs and pure cellulose acetate membrane was calculated to be 674.5019 $m^2\ g^{-1}$, 110.9820 $m^2\ g^{-1}$ and 13.9501 $m^2\ g^{-1}$, respectively (Fig. S16–S18, ESI†). These results indicated that the addition of **CJLU-1** increased the specific surface area of the cellulose acetate membrane.

The fabricated **CJLU-1** MMMs inherited the strong fluorescence of **CJLU-1** and exhibited blue fluorescence emission located at 454 nm (Fig. 5c and Fig. S19, ESI†). To demonstrate the feasibility of the fabricated MMMs as an effective sensing platform, **CJLU-1** MMMs were employed to detect nitroaromatic molecules in the vapor phase. Impressive fluorescence quenching was observed upon exposing nitroaromatic molecules, such as nitrobenzene, 2-nitrotoluene and PNP (Fig. S20–S22, ESI†). The fluorescence intensity of **CJLU-1** MMMs significantly decreased when they were exposed to nitrobenzene vapor for a very short time (30 s). And the fluorescence intensity gradually decreased with time, when the **CJLU-1** MMMs were exposed to nitrobenzene vapor for 5 min, the quenching efficiency (defined as $(I_0 - I)/I_0 \times 100$) reached 95% (Fig. 5a and b). After the **CJLU-1** MMMs were exposed to nitrobenzene vapor for 30 min, the white **CJLU-1** MMMs changed to light yellow, and the membrane's fluorescence was darkened from blue under 365 nm ultraviolet light irradiation (Fig. 5c). While for PNP, the fluorescence intensity showed a less quenching efficiency of 25% for a 60 min exposure time, which is due to its lower vapor pressure and therefore limited interaction with MMMs, reducing its impacts (Fig. S20, ESI†). For PA, the liquid detection experiment was carried out due to the very low concentration of the original PA solution (0.122% PA aqueous solution). The fluorescence intensity significantly decreases after the addition of 50 μL PA solution onto the membrane (Fig. S22, ESI†). In addition, after the addition of a drop of liquid such as 2,4-DNT, 2,6-DNT, NB, PNP and PA with certain concentration, the fluorescence colors of the **CJLU-1** MMMs darken from blue for a different degree under the illumination of 365 nm ultraviolet light (Fig. 5d), highlighting the straightforward and facile detection of nitroaromatic molecules by the MOF MMM approach.

To further investigate the practical utility of **CJLU-1** MMMs, the recovery and reproducibility of the membrane were determined. The fluorescence intensity of **CJLU-1** MMMs at 454 nm was quenched upon exposure to nitrobenzene vapor for 5 min, then the **CJLU-1** MMMs were immersed in ethanol for 5 min to wash off nitrobenzene on the membrane and dried naturally in air, and the fluorescence intensity of the **CJLU-1** MMMs can be recovered (Fig. 6). Even when the **CJLU-1** MMMs were reused for five cycles, the recovered fluorescence intensity can largely remain stable (Fig. 6). The superior reversible sensing performances demonstrate the feasibility of the **CJLU-1** MMMs for practical sensing applications.

Experimental

Synthesis of CJLU-1 nanoflowers

4,4′,4″-Nitrilotribenzoic acid (H_3TCA) (94.25 mg, 0.250 mmol) and $ZrCl_4$ (0.0863 g, 0.370 mmol) were added to 10 mL of DMF in a 50 mL Teflon-lined stainless-steel autoclave, and after the mixture was dissolved, then concentrated HCl (10.75 mL, 100 equiv.) was added to the above mixture. After sonication for 10 minutes, the mixture was heated at 120 °C for 2 days. Then, the temperature of the mixture dropped to room

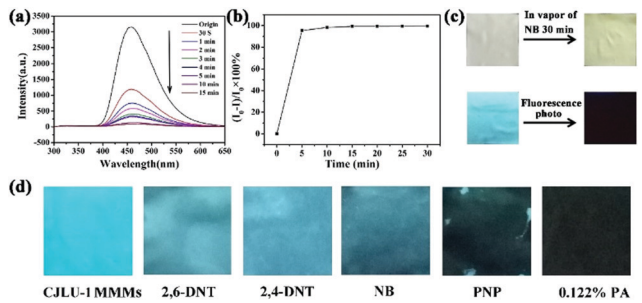

Fig. 5 (a) The emission of **CJLU-1** MMMs upon exposure to nitrobenzene vapor for different time periods; (b) quenching efficiency profile of **CJLU-1** MMMs upon exposure of NB as a function of time; (c) photo under nature light and 365 nm UV light of **CJLU-1** MMMs before and after exposure to NB for 30 min; and (d) fluorescence photos of **CJLU-1** MMMs after addition of 5 μL 0.1 M of nitroaromatics (the concentration of PA was 5.32×10^{-3} M) under 365 nm UV light.

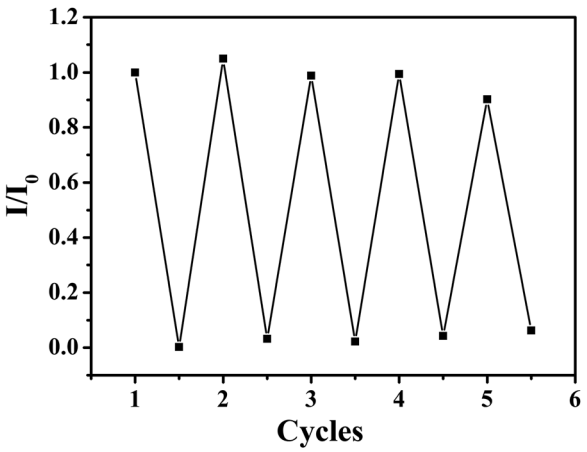

Fig. 6 The reversibility of the **CJLU-1** MMM test.

temperature and it was washed with DMF and methanol several times, respectively. And then, white powder was obtained.

Organic small molecule sensing

For an organic small molecule sensing experiment, 10 mg sample powder was added to 100 mL ethanol and sonicated for 20 minutes to obtain a suspension of **CJLU-1**. The luminescence sensing experiment was carried out by adding 50 μL of DMF, acetone, phenol, H_2O, aniline, toluene, NB, 2,4-DNT, 2,6-DNT, PNP (*p*-nitrophenol) and 1.22% PA (among them, the concentration of 1.22% PA was 5.32×10^{-2} M) with a concentration of 0.1 M to 2 mL suspension of **CJLU-1**, respectively.

Fabrication of CJLU-1 MMMs

200 mg of cellulose acetate was added to 1.8 g of acetone/DMF (mass/mass = 2/1), and sonication was carried out for 5 hours to dissolve the cellulose acetate to obtain casting solution. And then 120 mg of **CJLU-1** was added to the above casting solution to form a homogeneous solution by sonication. Then, the casting solution with **CJLU-1** was cast onto a glass plate using a wiper and immersed in deionized water to separate the composite film from the glass plate. After drying at room temperature, 1×1 cm^2 was cut from **CJLU-1** MMMs for the sensing test.

Vapor sensing of nitroaromatics

Take nitrobenzene for example; 2 mL of nitrobenzene was placed in a 20 mL sample vial, which was placed in a closed reagent bottle and allowed to stand for a few days to bring the nitrobenzene to equilibrium vapor pressure. A 1×1 cm^2 **CJLU-1** MMM was placed above the reagent bottle to expose it to nitrobenzene vapor. After a certain period of time, the slide was removed from the reagent bottle and its emission spectrum was collected immediately. The experimental details of other nitroaromatics are provide in the ESI.

Conclusions

To summarize, we have targeted a new luminescent flower-like metal-organic framework composed of ultra-thin nanosheet material **CJLU-1** ($Zr_6(\mu_3\text{-}O)_4(\mu_3\text{-}OH)_4(OH)_6(TCA)_2(H_2O)_6$) ($H_3TCA$ = tricarboxylic acids 4,4′,4″-nitrilotribenzoic acid) for the highly sensitive sensing of nitroaromatic molecules with fast response. The excellent luminescence sensing performance of the nanoflower material mainly comes from the rational design of an electron-donating triphenylamine ligand and the nanoflower structure with highly accessible active sites on the surface. The **CJLU-1** nanoflower material shows a high detection limit of 0.362 μM (≈83 ppb) toward PA, strong anti-interference and a fast response within seconds. Moreover, a novel sensing platform was established by hybridization of the **CJLU-1** nanoflower and cellulose acetate polymer into MMMs, and exhibits effective and reversible vapor sensing towards nitroaromatic molecules. This work suggests a promising route to develop novel nanostructured MOF probes and MOF-based MMMs as a nitroaromatic sensing platform with superior mechanical strength, flexibility and sensitivity towards practical sensing applications.

Conflicts of interest

There are no conflicts to declare.

Acknowledgements

This work was supported by the Natural Science Foundation of Zhejiang Province (No. LY19E020007 and LY20E020001), the National Natural Science Foundation of China (51672251) and the Fundamental Research Funds for the Provincial Universities of Zhejiang.

Notes and references

1 Y. Cui, Y. Yue, G. Qian and B. Chen, *Chem. Rev.*, 2012, **112**, 1126–1162.
2 M. Ding, R. W. Flaig, H.-L. Jiang and O. M. Yaghi, *Chem. Soc. Rev.*, 2019, **48**, 2783–2828.
3 D. J. Wales, J. Grand, V. P. Ting, R. D. Burke, K. J. Edler, C. R. Bowen, S. Mintova and A. D. Burrows, *Chem. Soc. Rev.*, 2015, **44**, 4290–4321.
4 S.-N. Zhao, X.-Z. Song, S.-Y. Song and H.-J. Zhang, *Coord. Chem. Rev.*, 2017, **337**, 80–96.
5 J. Gao, X. Qian, R. Lin, R. Krishna, H. Wu, W. Zhou and B. Chen, *Angew. Chem., Int. Ed.*, 2020, **59**, 4396–4400.
6 H. Xu, S. Sommer, N. L. B. Nyborg, J. Gao and B. B. Iversen, *Chem. – Eur. J.*, 2019, **25**, 2051–2058.
7 J. Gao, Q. Huang, Y.-Q. Lan and B. Chen, *Adv. Energy Sustainability Res.*, 2021, **2**, 2100033.
8 L. E. Kreno, K. Leong, O. K. Farha, M. Allendorf, R. P. Van Duyne and J. T. Hupp, *Chem. Rev.*, 2012, **112**, 1105–1125.
9 Y. Zhang, S. Yuan, G. Day, X. Wang, X. Yang and H.-C. Zhou, *Coord. Chem. Rev.*, 2018, **354**, 28–45.
10 L. Wang, H. Xu, J. Gao, J. Yao and Q. Zhang, *Coord. Chem. Rev.*, 2019, **398**, 213016.
11 W. P. Lustig, S. Mukherjee, N. D. Rudd, A. V. Desai, J. Li and S. K. Ghosh, *Chem. Soc. Rev.*, 2017, **46**, 3242–3285.
12 W.-M. He, Z. Zhou, Z. Han, S. Li, Z. Zhou, L.-F. Ma and S.-Q. Zang, *Angew. Chem., Int. Ed.*, 2021, **60**, 8505–8509.
13 J. Dong, A. K. Tummanapelli, X. Li, S. Ying, H. Hirao and D. Zhao, *Chem. Mater.*, 2016, **28**, 7889–7897.
14 Y. Guo, X. Feng, T. Han, S. Wang, Z. Lin, Y. Dong and B. Wang, *J. Am. Chem. Soc.*, 2014, **136**, 15485–15488.
15 L. Wang, J. Gao and J. Xu, *Sens. Actuators, B*, 2019, **293**, 71–82.
16 E. A. Dolgopolova, A. M. Rice, C. R. Martin and N. B. Shustova, *Chem. Soc. Rev.*, 2018, **47**, 4710–4728.
17 I. Stassen, N. Burtch, A. Talin, P. Falcaro, M. Allendorf and R. Ameloot, *Chem. Soc. Rev.*, 2017, **46**, 3185–3241.
18 M. Zhao, Y. Wang, Q. Ma, Y. Huang, X. Zhang, J. Ping, Z. Zhang, Q. Lu, Y. Yu and H. Xu, *Adv. Mater.*, 2015, **27**, 7372–7378.

19 R. Xu, Y. Wang, X. Duan, K. Lu, D. Micheroni, A. Hu and W. Lin, *J. Am. Chem. Soc.*, 2016, **138**, 2158–2161.
20 Y.-Z. Li, Z.-H. Fu and G. Xu, *Coord. Chem. Rev.*, 2019, **388**, 79–106.
21 S. Gbadamasi, M. Mohiuddin, V. Krishnamurthi, R. Verma, M. W. Khan, S. Pathak, K. Kalantar-Zadeh and N. Mahmood, *Chem. Soc. Rev.*, 2021, **50**, 4684–4729.
22 H. Xu, Y. Dong, Y. Wu, W. Ren, T. Zhao, S. Wang and J. Gao, *J. Solid State Chem.*, 2018, **258**, 441–446.
23 M. Zhao, Y. Huang, Y. Peng, Z. Huang, Q. Ma and H. Zhang, *Chem. Soc. Rev.*, 2018, **47**, 6267–6295.
24 H. Xu, J. Gao, X. Qian, J. Wang, H. He, Y. Cui, Y. Yang, Z. Wang and G. Qian, *J. Mater. Chem. A*, 2016, **4**, 10900–10905.
25 J. Dong, K. Zhang, X. Li, Y. Qian, H. Zhu, D. Yuan, Q.-H. Xu, J. Jiang and D. Zhao, *Nat. Commun.*, 2017, **8**, 1–14.
26 A. K. Chaudhari, H. J. Kim, I. Han and J. C. Tan, *Adv. Mater.*, 2017, **29**, 1701463.
27 X. Wang, Z. Jiang, C. Yang, S. Zhen, C. Huang and Y. Li, *J. Hazard. Mater.*, 2022, **423**, 126978.
28 F.-L. Li, P. Wang, X. Huang, D. J. Young, H.-F. Wang, P. Braunstein and J.-P. Lang, *Angew. Chem., Int. Ed.*, 2019, **58**, 7051–7056.
29 G. Lan, Z. Li, S. S. Veroneau, Y.-Y. Zhu, Z. Xu, C. Wang and W. Lin, *J. Am. Chem. Soc.*, 2018, **140**, 12369–12373.
30 Y. Ding, Y.-P. Chen, X. Zhang, L. Chen, Z. Dong, H.-L. Jiang, H. Xu and H.-C. Zhou, *J. Am. Chem. Soc.*, 2017, **139**, 9136–9139.
31 Y. Li, M. Lu, Y. Wu, Q. Ji, H. Xu, J. Gao, G. Qian and Q. Zhang, *J. Mater. Chem. A*, 2020, **8**, 18215–18219.
32 L. Cao, Z. Lin, W. Shi, Z. Wang, C. Zhang, X. Hu, C. Wang and W. Lin, *J. Am. Chem. Soc.*, 2017, **139**, 7020–7029.
33 T. Singha Mahapatra, A. Dey, H. Singh, S. S. Hossain, A. K. Mandal and A. Das, *Chem. Sci.*, 2020, **11**, 1032–1042.
34 V. K. Maka, A. Mukhopadhyay, G. Savitha and J. N. Moorthy, *Nanoscale*, 2018, **10**, 22389–22399.
35 C.-X. Yu, F.-L. Hu, J.-G. Song, J.-L. Zhang, S.-S. Liu, B.-X. Wang, H. Meng, L.-L. Liu and L.-F. Ma, *Sens. Actuators, B*, 2020, **310**, 127819.
36 A. Betard and R. A. Fischer, *Chem. Rev.*, 2012, **112**, 1055–1083.
37 M. S. Denny, J. C. Moreton, L. Benz and S. M. Cohen, *Nat. Rev. Mater.*, 2016, **1**, 1–17.
38 T. Kitao, Y. Zhang, S. Kitagawa, B. Wang and T. Uemura, *Chem. Soc. Rev.*, 2017, **46**, 3108–3133.
39 J. Dechnik, J. Gascon, C. J. Doonan, C. Janiak and C. J. Sumby, *Angew. Chem., Int. Ed.*, 2017, **56**, 9292–9310.
40 L. Xiang, L. Sheng, C. Wang, L. Zhang, Y. Pan and Y. Li, *Adv. Mater.*, 2017, **29**, 1606999.
41 B. Seoane, J. Coronas, I. Gascon, M. E. Benavides, O. Karvan, J. Caro, F. Kapteijn and J. Gascon, *Chem. Soc. Rev.*, 2015, **44**, 2421–2454.
42 Y. Peng, Y. Li, Y. Ban and W. Yang, *Angew. Chem., Int. Ed.*, 2017, **56**, 9757–9761.
43 T. Feng, Y. Ye, X. Liu, H. Cui, Z. Li, Y. Zhang, B. Liang, H. Li and B. Chen, *Angew. Chem., Int. Ed.*, 2020, **59**, 21752–21757.
44 Y. Ding, Y. Lu, K. Yu, S. Wang, D. Zhao and B. Chen, *Adv. Opt. Mater.*, 2021, **9**, 2100945.
45 M. Kalaj, K. C. Bentz, S. Ayala Jr, J. M. Palomba, K. S. Barcus, Y. Katayama and S. M. Cohen, *Chem. Rev.*, 2020, **120**, 8267–8302.
46 T.-T. Li, L. Liu, M.-L. Gao and Z.-B. Han, *Chem. Commun.*, 2019, **55**, 4941–4944.
47 Q.-Y. Li, Y.-A. Li, Q. Guan, W.-Y. Li, X.-J. Dong and Y.-B. Dong, *Inorg. Chem.*, 2019, **58**, 9890–9896.
48 X. Zhang, Q. Zhang, D. Yue, J. Zhang, J. Wang, B. Li, Y. Yang, Y. Cui and G. Qian, *Small*, 2018, **14**, 1801563.
49 J. Gao, Y. Cai, X. Qian, P. Liu, H. Wu, W. Zhou, D.-X. Liu, L. Li, R.-B. Lin and B. Chen, *Angew. Chem., Int. Ed.*, 2021, **60**, 20400–20406.
50 Z. Hu, B. J. Deibert and J. Li, *Chem. Soc. Rev.*, 2014, **43**, 5815–5840.
51 S. S. Nagarkar, B. Joarder, A. K. Chaudhari, S. Mukherjee and S. K. Ghosh, *Angew. Chem., Int. Ed.*, 2013, **52**, 2881–2885.
52 L. Chu, X. Zhang, W. Niu, S. Wu, W. Ma, B. Tang and S. Zhang, *J. Mater. Chem. C*, 2019, **7**, 7411–7417.
53 W. Ren, J. Gao, C. Lei, Y. Xie, Y. Cai, Q. Ni and J. Yao, *Chem. Eng. J.*, 2018, **349**, 766–774.
54 S. Wang, F. Li, X. Dai, C. Wang, X. Lv, G. I. Waterhouse, H. Fan and S. Ai, *J. Hazard. Mater.*, 2020, **384**, 121417.
55 Y. Wu, Y. Xie, F. Zhong, J. Gao and J. Yao, *Microporous Mesoporous Mater.*, 2020, **306**, 110386.